Simulations of high-gain shock-ignited inertial-confinement-fusion implosions using less than 1 MJ of direct KrF laser energy

Jason W. Bates*[,a], Andrew J. Schmitt[a], David E. Fyfe[b], Steve P. Obenschain[a], Steve T. Zalesak[a]

[a] *Plasma Physics Division, U.S. Naval Research Laboratory, Washington, DC 20375*
[b] *Laboratory for Computational Physics and Fluid Dynamics, U.S. Naval Research Laboratory, Washington, DC 20375*

Abstract

In this paper, we report on recent numerical simulations of inertial-confinement-fusion (ICF) implosions using the FAST radiation hydro-code at the U.S. Naval Research Laboratory. Our study focuses on three classes of shock-ignited target designs utilizing less than 1 MJ of direct KrF laser energy, which was "zoomed" to maximize the coupling efficiency. In the shock-ignition approach [R. Betti, C.D. Zhou, K.S. Anderson, *et al.*, Phys. Rev. Lett. **98**, 155001 (2007)], a moderate-intensity, compressive laser pulse is followed by a short-duration high-intensity spike that launches a spherically-convergent shock wave to ignite a thick shell of compressed fuel. Such an arrangement appears to offer several significant advantages, including a low ignition threshold, high gain, and less susceptibility to the deleterious effects of hydrodynamic and laser-plasma instabilities. According to one-dimensional simulations, fusion gains over 200 can be achieved with shock-ignited targets using less than 750 kJ of laser energy. This represents a significant improvement in performance over conventional centrally-ignited designs. To examine the stability of these targets, several two-dimensional simulations were also performed that incorporated realistic perturbation sources such as laser imprinting and roughness spectra for inner/outer pellet surfaces. Although the simulations indicate that appreciable low-mode distortion of the fuel shell can occur at late time as a result of these perturbations, high gains are still achieved in many cases owing to the low in-flight aspect ratios of shock-ignited targets. We should remark, though, that the high convergence ratios of these same designs suggest that other sources of low-mode asymmetries, which were not considered in this study (*e.g.*, beam misalignment and energy-balance errors), may be important in determining overall pellet stability and performance. We discuss these issues, as well as other salient design considerations for shock-ignited ICF targets.

Key words: Shock ignition, Direct-drive laser fusion, ICF target designs, KrF lasers
PACS: 52.57.-z, 52.57.Bc, 52.57.Fg

1. Introduction

The standard direct-drive approach to inertial confinement fusion (ICF) involves illuminating a millimeter-size pellet containing a frozen mixture of deuterium and tritium (DT) with many intense beams of laser light. The energy deposited by the lasers rapidly ablates the outer surface of the spherical pellet, which compresses the underlying DT fuel and accelerates it inward to high velocity via the "rocket effect" [1]. Substantial nuclear fusion reactions can occur if, upon stagnation, the compressed fuel shell achieves a density on the order of 1000 times that of solid DT and the temperature of the central hot-spot reaches several thousand electron volts [2]. To overcome the low overall efficiencies inherent in ICF scenarios, the energy gain of an implosion must (on average) exceed a value of 100 for any commercial application of fusion power to be practical economically. Previously, it was estimated that a few megajoules of laser energy were required to satisfy this requirement [3]. A novel variation of the direct-drive scheme known as shock ignition [4, 5], however, suggest that high fusion gains may be possible for significantly lower laser energies.

In conventional direct-drive designs, the high-intensity portion of the laser pulse performs the double duty of both compressing the fuel to large density and forming the central hot spot that triggers ignition. To do this, the fuel shell must be driven inward at high velocity (typically $350 - 400\,km/s$). In contrast, the

*Corresponding author: jason.bates@nrl.navy.mil

laser pulse for shock-ignited targets is designed to separate the compression and ignition stages of the implosion by using a moderate-intensity pulse followed by a short-duration high-intensity spike. The latter launches a spherically-convergent shock wave into the target to ignite the core of compressed fuel. Because the implosion velocity of the shell is significantly less than that required for conventional central-hot-spot ignition ($\sim 250\,km/s$), thicker targets containing more fuel mass can be assembled for the same kinetic energy. In theory, this allows for the possibility of achieving high gains at low driver energies, provided ignition occurs.

To explore the utility of the shock ignition approach for direct-drive laser fusion, a numerical study was recently conducted at the U.S. Naval Research Laboratory (NRL) employing the multidimensional "rad-hydro" code known as FAST [6]. This code models the physical processes relevant to ICF pellet implosions by solving the equations of radiative hydrodynamics, including the effects of laser absorption, nonlinear thermal transport, and thermonuclear burn. Using FAST, three classes of shock-ignited targets were designed that achieve one-dimensional fusion-energy gains in the range $\sim 100-200$ using less that $1\,MJ$ of direct KrF laser energy (see Fig. 1). It is important to note that such high gains are due in part to the unique capabilities of KrF drivers, which offer at least two significant advantages over Nd:glass lasers. First, the deep ultraviolet wavelength of KrF laser light ($0.248\,\mu m$) enhances performance through increased absorption in the coronal plasma surrounding the target. Second, the flexible focussing capabilities of KrF drivers permit the laser spot size to be "zoomed" twice during the implosion. Zooming means that the laser spot is reduced in size to more closely match that of the critical surface. This has the beneficial effect of minimizing the refractive losses by keeping the laser energy near the ablation surface and contributes to higher gains through improved coupling efficiencies.

The organization of this paper is as follows. In the next section, we present the details of the sub-MJ targets that were developed recently at NRL and explain the features of the KrF-laser pulses that were used to implode them. We also review in Sec. 2 the basic design procedure for shock-ignited pellets, which begins with an initial tuning of the laser pulse without the ignition spike being present. Once this is accomplished, the spike is added to the pulse shape and its parameters are systematically varied to find the combination that result in the highest gain — a process that usually requires the completion of hundreds of one-dimensional simulations for each class of designs. We discuss this

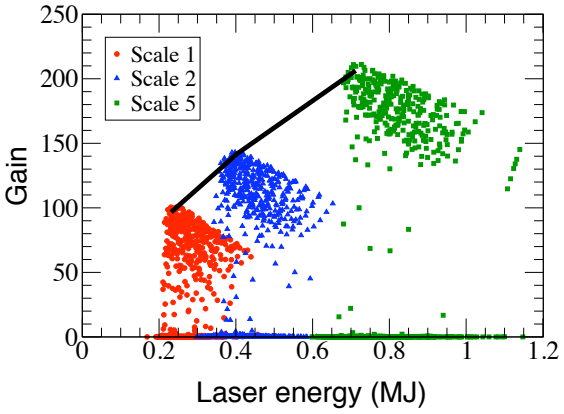

Figure 1: Results of one-dimensional simulations showing the fusion energy gain as a function of KrF laser energy for three classes of shock-ignited target designs. As explained in the text, the scale-1 target (red circles) serves as the baseline design in this study; the other two classes of pellets have total masses that are two and five times larger.

parameter search and show examples of the mutidimensional phase space that results. To examine the stability of these targets in the presence of realistic perturbation sources such as laser imprinting and roughness spectra for inner and outer pellet finishes, some two-dimensional simulations were also conducted, the results of which appear in Sec. 3. Finally, in Sec. 4, we state the conclusions of this investigation and briefly describe topics of interest for future work on shock-ignited targets. The reader should note that all three of the designs considered here were introduced previously in a different publication [7]. In that paper, however, only the properties of the smallest pellet were analyzed in detail. Here, our focus is on presenting some previously-unpublished simulation results for the two larger target classes.

2. Three Classes of Sub-MJ Shock-Ignited Designs

In this section, we describe three classes of shock-ignited targets that have been designed at NRL for KrF lasers. We use the term "class" in this paper to refer to a pellet of fixed size and composition, which is illuminated by a series of laser pulses with varying power and temporal parameters. The pellets differ in size and mass, but all three share the same basic material cross-section, a cutaway sketch of which appears in Fig. 2. The core of the pellet, which has a radius R_1, is filled with DT va-

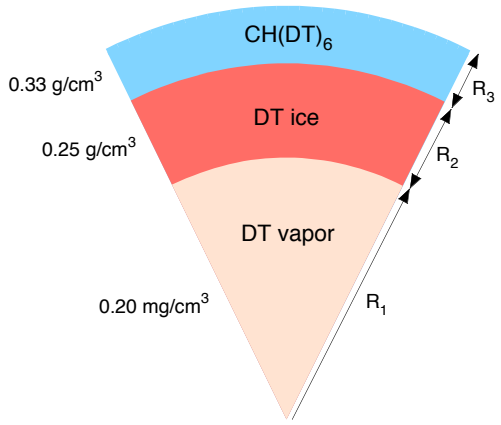

Figure 2: Generic cross-section of a shock-ignited pellet. The formula $CH(DT)_6$ denotes a $100\,mg/cm^3$ foam ablator wicked with DT and frozen. The shell dimensions R_1, R_2, and R_3 for each design class are listed in Table 1.

Parameter	Scale-1	Scale-2	Scale-5
Pellet mass (mg)	0.58	1.17	2.89
R_1 (μm)	512	640	871
R_2 (μm)	237	300	407
R_3 (μm)	108	136	177
Initial aspect ratio	2.48	2.47	2.49
Convergence ratio	64	65	63
Peak velocity (km/s)	286	260	220
Laser energy (kJ)	243	398	727
Highest gain	101	143	210

Table 1: Parameters for the three classes of shock-ignited pellets. The entries for convergence ratio, peak velocity, and laser energy in each design class correspond to the target that produced the highest gain.

por at a density of $0.20\,mg/cm^3$. Surrounding this core are two shells of solid material with dimensions R_2 and R_3. The first shell is a DT "ice" layer with a density of $0.25\,g/cm^3$, and the second is a $100\,mg/cm^3$-foam ablator into which DT has been wicked and frozen. The wicked foam, which is abbreviated as $CH(DT)_6$, has an overall density of $0.33\,g/cm^3$. In reality, there will also be a very thin ($\sim 5\,\mu m$) coating of polystyrene (CH) on the outer surface to provide structural integrity for the pellet and to act as a vapor barrier for the DT contained within; this layer is not expected to alter appreciably the performance of an implosion and is ignored here for computational simplicity. As shown in Fig. 1, the three designs utilize about 240, 400, and $730\,kJ$ of direct KrF laser energy and according to one-dimensional simulations, achieve peak fusion gains of approximately 100, 140, and 210, respectively. These results are tabulated in Table 1, along with the radii R_1, R_2, and R_3 of each material shell for all three designs.

The smallest target, which belongs to the scale-1 class, has a total mass of about $0.58\,mg$, and serves as the baseline for this investigation. As mentioned in the previous section, a detailed description of this target — as well as an analysis of its two-dimensional stability properties — has already been presented elsewhere [7]. The names of the two other classes, scale-2 and scale-5, are derived from the fact that their masses are two and five times larger, respectively, than that of the scale-1 design. (Note that the outer radii of the two larger targets vary approximately as mass to the one-third power.) Despite their size and mass differences, though, all three pellets were constructed to have roughly the same initial aspect ratio $(R_1 + R_2 + R_3)/(R_2 + R_3) \simeq 2.5$, which is significantly less than values associated with centrally-ignited designs [8]. Such low aspect ratios are a desirable property of direct-drive ICF targets since they imply a greater fuel-shell thickness to resist the deleterious effects of hydrodynamic instabilities during the implosion process.

In addition to lower aspect ratios, shock-ignition designs differ from their centrally-ignited counterparts in the shape of the laser pulses used to drive them. This difference is illustrated in Fig. 3, which shows a plot of the laser power versus time for the two schemes. The shock-ignition pulse is comprised of four basic components: a picket, a foot, the main drive, and an ignition spike, and is based on a profile proposed by Betti and coworkers [9]. For all of the target designs considered in this study, the laser pulse possesses the same basic structure as the one shown in Fig. 3, albeit with different power levels, temporal parameters, and total energy. We should point out that within each class of designs, the laser profiles are generally identical up until the start of the main drive section of the pulse It is the variation of the start time, power level, and duration of the main drive and ensuing ignition spike that account for the differences within each design class. As we shall see, high

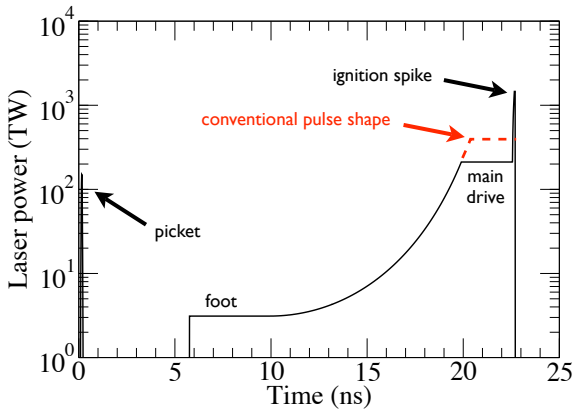

Figure 3: Plot of laser power versus time for one of the pulse shapes from the scale-5 design category (black curve). The pulse is based on a "double power-law" design by R. Betti [9] and is comprised of four distinct components: a picket, a foot, the main drive, and an ignition spike, whose various functions are explained in the text. Note that the dashed red curve denotes the pulse shape for a conventional, centrally-ignited target design, which has a main drive with a significantly greater power (and intensity) level than its shock-ignited counterpart.

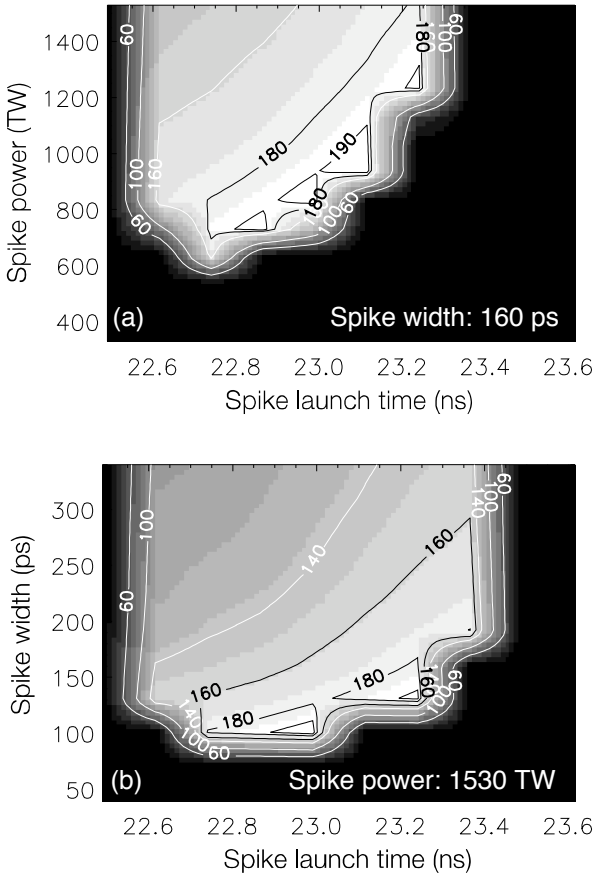

Figure 4: Examples of fusion-energy gain contours for a shock-ignited target. The gain of a target implosion is a function of many parameters and is especially sensitive to the power, duration, and launch time of the ignition spike. The two plots shown in this figure are two-dimensional "slices" through the three-dimensional space formed by the variation of these three quantities. Gain contours are plotted as a function of spike launch time versus (a) spike power and (b) spike width. Both examples are for a scale-5 design with a main-drive power of 210 TW.

gains can be achieved for a range of pulse parameters, and in general, the higher the power level (compression) of the main drive, the lower the spike energy needs to be to ignite the target.

Let us now turn to an explanation of the function of each laser-pulse component mentioned above and briefly describe the tuning process that is required to achieve high-gain shock-ignited implosions. The first component of the laser pulse is a leading-edge picket, which has a Gaussian shape and a fixed width of about 50 ps; its role is to rapidly compress and then rarefy the ablation layer of the pellet, and in so doing, it establishes an adiabat profile with a spatial variation that is high near the outside surface of the target, and low near the DT fuel. Such an arrangement is advantageous in that it helps to stabilize the implosion with respect to the ablative Richtmyer-Meshkov and Rayleigh-Taylor instabilities [10, 11]. After a quiescent period lasting for several nanoseconds, the laser power rises to form the foot pulse, whose amplitude is designed to launch a few-megabar shock wave into the target and set the adiabat to a value between 1 and 2 in the fuel layer; the start time of the foot pulse is chosen so that the shock it generates breaks out of the inner DT surface simultaneously with the one from the picket. Eventually, the foot pulse rises smoothly (according to a double power law [9]) over a period of many nanoseconds to reach the main drive. The criteria used to set the amplitude and rise time for this section of the laser pulse are twofold. First, the power level is chosen to accelerate the target to a velocity of about 250 km/s, which is not high enough to produce a sufficiently-hot central spark to trigger ignition. Then, the time at which the pulse reaches the main drive is varied iteratively to produce the highest compression as measured by the peak density, pressure, and areal mass of the non-ignited pellet. Note that the maximum intensity that occurs during the main drive is fairly low — about $1.5 \times 10^{15} W/cm^2$. Once the tuning of the main drive is complete, an ignition spike is added

Parameter	Scale-1	Scale-2	Scale-5
Picket power (TW)	36.3	64.0	161
Start of foot (ns)	2.35	3.60	5.75
Foot power (TW)	1.07	1.70	3.11
Start of main drive (ns)	10.7	14.3	20.6
Main drive power (TW)	95	110	120
Start of spike (ns)	11.9	16.0	23.3
Spike power (TW)	350	500	450
Spike width (ps)	250	250	500
Zooming fractions (%)	63/41	63/41	64/46
Peak Intensity (PW/cm^2)	14	10	5.9

Table 2: Laser-pulse parameters that resulted is the highest gain for each class of shock-ignited target designs.

to the end of the pulse profile. The three parameters that characterize the spike — its temporal width, power level, and start time — are then varied systematically by performing numerous one-dimensional simulations to generate gain contours, examples of which are presented in Fig. 4.

In addition to varying the parameters of the ignition spike, we also examined in this investigation the consequences of tuning the main-drive portion of the laser pulse. As a rule of thumb, the power level of the main-drive was selected in the initial stage of a design to produce an implosion velocity of roughly $250\,km/s$ in the absence of the ignition spike. In some cases, however, higher gains were obtained for somewhat lower velocities. This was true, for example, in the scale-5 target design, which achieved a peak gain of 210 for an implosion velocity of only $220\,km/s$ (see Table 1). Details of the laser pulse shapes that resulted in the highest gain for each design class are presented in Table 2.

Another important feature of the laser drive in this study is optical zooming, which is done twice during the pellet implosion. The first time a zoom occurs is at the start of the main drive, when the diameter of the critical surface is reduced to about 63% of its original size; the second time that the laser spot is zoomed is just as the ignition spike begins, when the critical-surface diameter is approximately 41% of the initial value. Zooming of the laser pulse is beneficial in that it helps to increase the coupling efficiency and generally leads to higher gain, but it also can exacerbate another issue: the high intensity levels inherent in shock-ignition schemes. With zooming, the intensity of the laser spot during the spike can reach values as high as $5\times10^{16}W/cm^2$. This is well above the threshold for laser-plasma instabilities such as stimulated Brillouin and Raman scattering and two plasmon decay — even for the short wavelength of KrF laser light modeled in this investigation.

The occurrence of laser-plasma instabilities in ICF targets has several undesirable consequences. These include a reduced absorption efficiency (due to an increase of reflected and scattered laser light) and the generation of super-thermal ("hot") electrons. In conventional centrally-ignited targets, hot electrons are extremely deleterious to the implosion process because they penetrate and heat the fuel shell, which reduces the final compression, and potentially spoils ignition. In shock-ignited designs, the situation is somewhat different in that the high-intensity portion of the laser pulse occurs only near the end of the implosion. At that late time, the areal density of the target is rising rapidly due to shock compression and spherical convergence effects, and can reach values in excess of $100\,mg/cm^2$. According to recent estimates [12, 13], this is sufficient to stop 100-keV electrons, which only have a ρR-range of about $17\,mg/cm^2$ in DT. We should point out, however, that it is currently unknown what the precise energy distribution of hot electrons is, in shock-ignition scenarios, and no attempt has been made to model the effects of their production or transport in any of the simulation results presented here.

3. Examples of Two-Dimensional Simulations

In this section, we explore the sensitivity of shock-ignited targets to realistic perturbation sources, including roughness spectra for inner and outer pellet finishes, as well as laser imprinting. Such perturbations are an important consideration in any ICF target-design process since they can grow to sufficient amplitudes during the implosion (due to the ablative Richtmyer-Meshkov and Rayleigh-Taylor instabilities) that the fusion energy gain is significantly reduced, or ignition is spoiled altogether. As an initial attempt to assess the stability of our shock-ignited pellets under perturbed conditions, we have performed two-dimensional simulations using the FAST code, examples of which are shown below for the scale-2 and scale-5 designs. We remind the reader

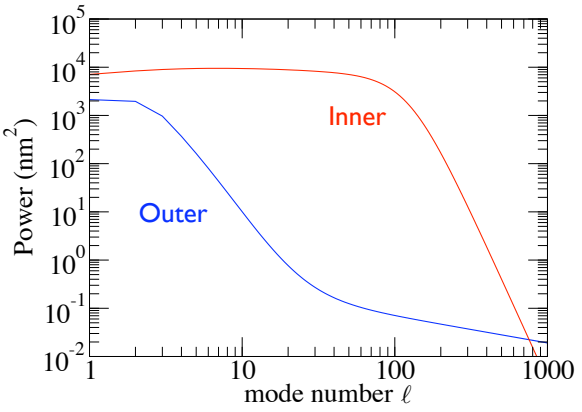

Figure 5: "NIF-like" power spectra of outer and inner surface perturbations. The outer surface spectrum (blue curve) is highly peaked at the lowest mode numbers (longest wavelengths) and has 90% of its power in modes $\ell \lesssim 10$. In contrast, the bulk of contributions for inner surface perturbations (red curve) come from modes $10 \lesssim \ell \lesssim 200$. Note that the $\ell = 1$ mode was not seeded for either perturbation in our simulations.

that a stability analysis of the scale-1 target has already been presented in Ref. [7].

The power spectra for inner and outer surface perturbations that were used in this study are plotted in Fig. 5 as a function of spherical mode number ℓ. Note, however, that the $\ell = 1$ mode was not seeded in any of our simulations. The curves in this figure were generated using a "NIF-spec" surface-finish standard [14, 15], but with the outer perturbation spectrum altered to have smaller amplitudes at low modes ($\ell \leq 4$). Even with this modification, though, the spectrum is still highly peaked at the lowest mode numbers (longest wavelengths), and has 90% of its power in modes $2 \lesssim \ell \lesssim 10$. The mode amplitude $r_{\ell m}$ has the analytical form:

$$r_{\ell m}(nm) = \begin{cases} 102 - 4.8\,(\ell - 1.8)^{2.4} & \ell < 5 \\ 9600\,\ell^{-3.39} + 2.4\,\ell^{-0.78} & \ell \geq 5. \end{cases} \quad (1)$$

In contrast, the bulk of contributions for inner surface perturbations come from a much broader range ($2 \lesssim \ell \lesssim 100$), and are modeled by the expression

$$r_{\ell m}\,(nm) = \frac{1000}{3\,\ell^{0.6} + 2.2 \times 10^{-7}\,\ell^4}\,. \quad (2)$$

Note that the curves appearing in Fig. 5 are the two-dimensional power spectra P_{2D} for the mode amplitudes given above, where $P_{2D} = (2\,\ell + 1)^2\, r_{\ell m}^2 / 4\,\pi$. We should also point out that the standard, net root-mean-square amplitude for outer perturbations is $1/8\,\mu m$ in CH. Since we have ignored the CH cover layer in our simulations, however, we scale this value to find the equivalent perturbation (in an areal-mass sense) for the DT-wicked foam. This is done by multiplying the original amplitude by the density ratio of the two materials, which yields $1/8\,\mu m \times (1.07/0.33) = 0.41\,\mu m$. The net root-mean-square amplitude for inner perturbations is nominally $1\,\mu m$.

Let us now examine the results of some two-dimensional FAST simulations that were run using the above surface-roughness spectra, as well as a model for induced-spatial-incoherence (ISI) laser non-uniformity of 300 overlapped beams with a bandwidth of 1 THz [16, 17]. The computational grid for our calculations used between 840 and 1000 points in the radial direction and 2048 points in polar angle from pole-to-pole, so that modes with $\ell = 2 - 512$ were resolved (assuming 8 points per wavelength are sufficient to do so). These high-resolution simulations typically required several days of run time to complete using 32 nodes of a distributed-memory computing facility at NRL, in which each node is comprised of dual, quad-core, Intel Xeon processors.

The results of our first high-resolution simulation are presented in Fig. 6. The plots in this figure show the relative mass density of a scale-2 target at six different times during an implosion in which all three sources of non-uniformity were present simultaneously. Although high-frequency perturbations are visible soon after the launch of the ignitor shock at $t = 16.45\,ns$, the structure of the pellet at stagnation ($t = 16.94\,ns$) is clearly dominated by a low-mode distortion ($\ell \sim 5$). Despite the lack of symmetry at the end of the implosion, however, the fuel still ignites and significant thermonuclear burn occurs; the fusion energy gain in this example is 103, which is a reduction of only 29 % from the maximum one-dimensional result achieved in the same design category (see Table 1).

Additional two-dimensional simulations of shock-ignited target implosions appear in Fig. 7. In these examples, only inner and outer surface non-uniformities were considered and the objective was to determine the effect of perturbations with amplitudes that were appreciably larger than the nominal values quoted above. The plots in this figure contain results from three different simulations of scale-5 target implosions, which are presented at two different times: after the launch of the ignition shock (top row), and as burn begins (bottom row). The first column of plots corresponds to a case in which only outer surface perturbations, with a root-mean-square amplitude of $0.41\,\mu m$ at the start of the calculation, were present; the second column show

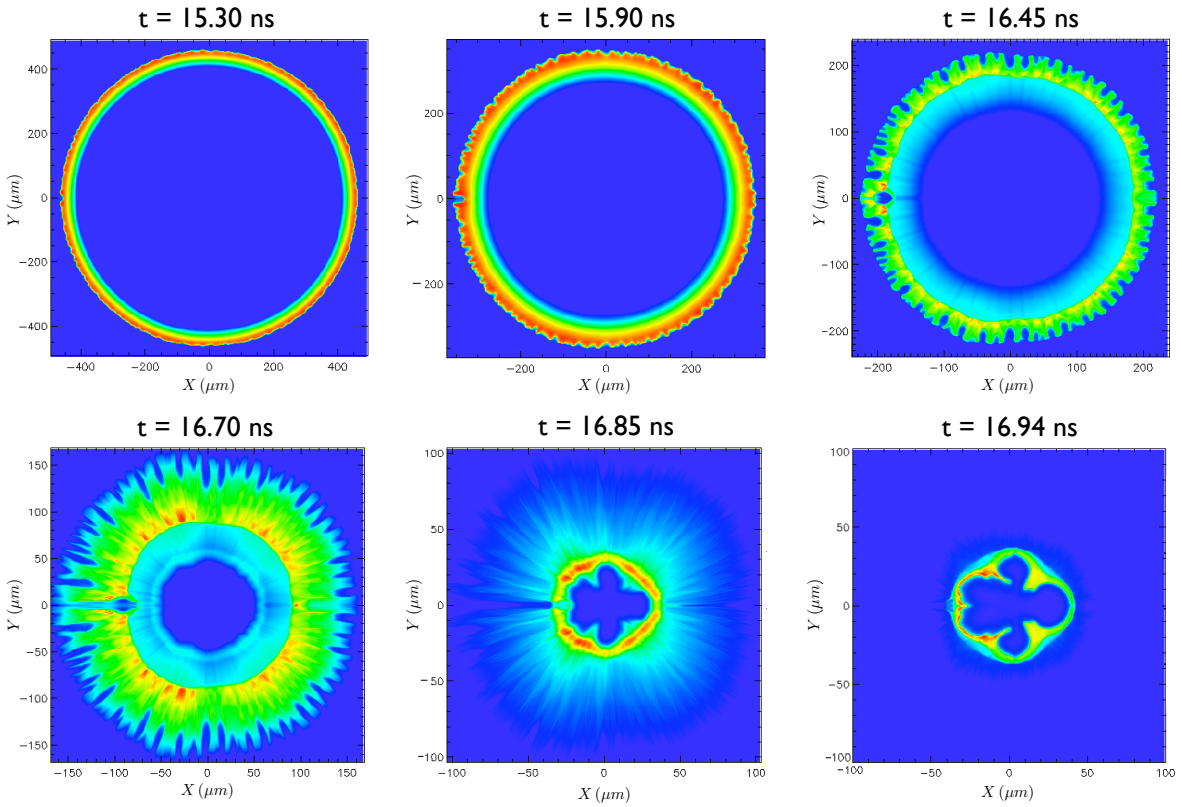

Figure 6: Density color plots from a 2D FAST simulation of a scale-2 target implosion. In this example, all three sources of perturbations (outer and inner NIF-like surface finishes, as well as 1-THz, 300-beam, ISI laser non-uniformity) are present simultaneously. The ignition spike has a power of 675, TW and a duration of 450 ps. A fusion energy gain of 103 is achieved.

the results of an implosion for an initial amplitude that was twice that value. In both cases, gains in excess of 175 were achieved using an ignition spike with a power of 700 TW and a width of 500 ps. The third column of plots in Fig. 7 shows a simulation with inner surface perturbations only, but with an amplitude that is initially three times the NIF standard (3 μm). The distortion of the pellet is dominated by a higher-frequency perturbation than in the other two cases, which is perhaps not too surprising given the broad inner-surface spectrum (see Fig. 5). This pellet also performs well, releasing over 160 MJ of fusion energy for a gain of 173.

4. Conclusions

In this paper, we have reported on recent numerical simulations of ICF pellet implosions using the FAST radiation-hydrocode at NRL. We discussed three classes of target designs based on a shock-ignition concept proposed by Betti and others [5] for direct-drive laser fusion. All three of the designs considered in this paper utilize less than 1MJ of KrF laser light and achieve one-dimensional fusion-energy gains between 100 and 200. It is important to note that these results are predicated, in part, on the special properties of KrF laser drivers, which include a deep ultraviolet wavelength (0.248 μm) and flexible focussing capabilities. The former enhances target performance through increased absorption in the under-dense plasma surrounding the pellet, while the latter allows the laser spot to be shrunk (zoomed) twice during the implosion to the size of the critical surface. This has the benefit of reducing the refractive losses and couples more of the laser light into the target, which minimizes the energy required to achieve high gains.

For each class of designs considered in this investigation, extensive searches were performed to find the optimum laser-pulse shape to implode the pellet. This was done using a one-dimensional version of FAST and the varied quantities were the spike power, its duration and start time, and the amplitude of the main drive. Hundreds, and sometimes thousands, of simu-

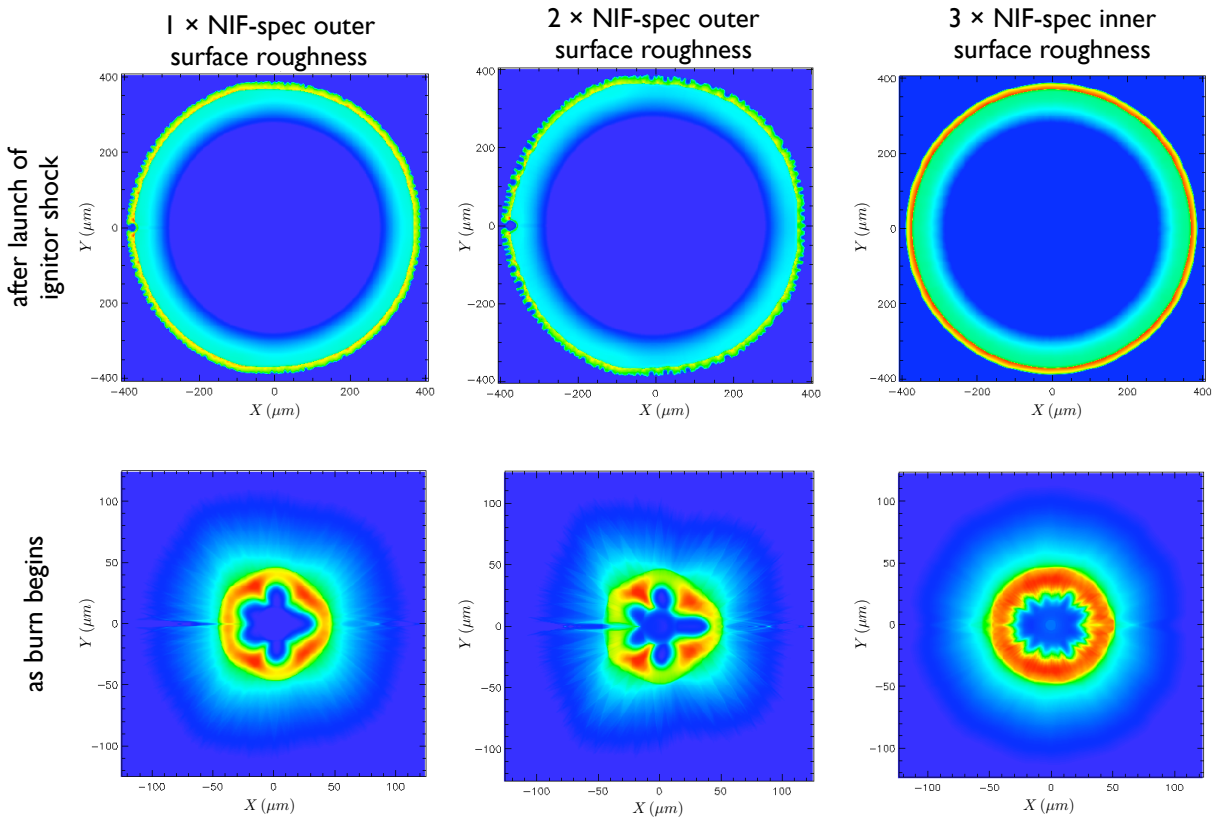

Figure 7: Density color plots from a 2D FAST simulation of a scale-5 target implosion. In this example, results from three different simulations are shown at two different times: after the launch of the ignition shock (top row), and as burn begins (bottom row).

lations were required in each design class to map the space of fusion energy gain formed by a modest variation of these parameters. The results of this exercise indicate that laser-pulse timing and intensity requirements are generally within acceptable ranges to achieve high-gain shock-ignited implosions. Another conclusion from this section of our study is that during the ignition spike, the pulse intensity reaches sufficiently high levels that super-thermal electrons likely will be produced in the corona by laser-plasma instabilities, but the consequences of this process for shock ignition is presently unclear. It is possible, for example, that the areal mass of the target at the final stages of the implosion is high enough that hot electrons are completely absorbed on the surface of the fuel shell; such a scenario could actually *help* to enhance the drive of the ignitor shock, but further research will be required to elucidate how energetic and numerous the electrons generated by laser-plasma instabilities are under shock-ignition conditions. We wish to emphasize that we have not attempted to model the effects of such instabilities in any of the designs presented in this paper.

To examine the hydrodynamic stability of shock-ignited targets in the presence of realistic perturbation sources, some two-dimensional simulations were also conducted in this investigation using the FAST code. We considered inner and outer surface irregularities, as well as broad-band laser non-uniformities. We found that each perturbation source (considered individually at its nominal level) resulted in only a modest degradation of target performance. The first example that we presented was a scale-2 target implosion in which all three sources of perturbations were present *simultaneously*. In that case, a fusion energy gain of 103 was obtained, which is only 29 % less than the maximum one-dimensional value achieved in the same design class. We also showed results from two-dimensional simulations of the scale-5 target, which included outer and inner surface perturbations with root-mean-square amplitudes that were two and three times higher, respectively,

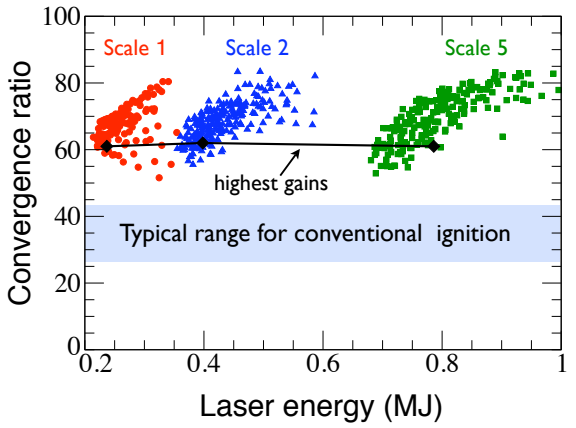

Figure 8: Convergence ratios for the three classes of shock-ignited pellet designs considered in this paper.

than the NIF-spec values. Although the simulations indicate that appreciable distortion of the fuel shell can occur at late time as a result of such perturbations, high gains were still achieved in these examples. This is due, at least in part, to the thicker fuel shells associated with low-aspect-ratio designs, which are better able to resist the growth of hydrodynamic instabilities that occur during the implosion process.

While a low aspect ratio is a geometric feature that bodes well for shock-ignited pellets, there is another physical property of these same designs that may not be very beneficial for target performance, namely, a high convergence ratio. Figure 8 show a plot of this quantity (as measured by the initial pellet radius divided by that of the spark) as a function of laser energy. Note that the highest-gain pellet in each design class has a convergence ratio of about 60, which is considerably greater than values typically associated with conventional direct-drive targets. These results imply that a shock-ignited pellet likely will be more sensitive to beam misalignment and energy-balance errors than its centrally-ignited counterpart, since the imploding fuel shell must converges to a smaller final volume. Such errors in alignment and energy balance are represented by low-mode contributions to the laser non-uniformity spectrum —- perturbations that were *not* modeled in the two-dimensional simulations presented in this paper. In the future, it will be important to address the impact of these perturbation sources on target performance.

Acknowledgments

This work was performed under the auspices of the U.S. Department of the Energy. The authors are grateful to Keith Obenschain for assistance with the computing facilities at NRL.

References

[1] J.J. Duderstadt and G.A. Moses, *Inertial Connement Fusion* (Wiley, New York, 1982).
[2] S. Atzeni and J. Meyer-ter-Vehn, *The Physics of Inertial Fusion* (Clarendon Press, Oxford, 2004).
[3] S.E. Bodner, D.G. Colombant, J.H. Gardner, R.H. Lehmberg, S.P. Obenschain, L. Phillips, A.J. Schmitt, J.D. Sethian, R.L. McCrory, W. Seka, C.P. Verdon, J.P. Knauer, B.B. Afeyan, H.T. Powell, Phys. Plasmas **5**, 1901 (1998).
[4] V.A. Shcherbakov, Sov. J. Plasma Phys. **9**, 240 (1983).
[5] R. Betti, C.D. Zhou, K.S. Anderson, L.J. Perkins, W. Theobold, A.A. Solodov, Phys. Rev. Lett. **98**, 155001 (2007).
[6] J. H. Gardner, A.J. Schmitt, J.P. Dahlburg, C.J. Pawley, S.E. Bodner, S.P. Obenschain, V. Serlin, Y. Aglitskiy, Phys. Plasmas **5**, 1935 (1998).
[7] A.J. Schmitt, J.W. Bates, S.P. Obenschain, S.T. Zalesak, D.E. Fyfe, R. Betti, Fusion Sci. and Tech. **56**, 377 (2009).
[8] S.E. Bodner, D.G. Colombant, A.J. Schmitt, M. Klapish, Phys. Plasmas **7**, 2298 (2000).
[9] R. Betti, K. Anderson, J. Knauer, T.J.B. Collins, R.L. McCrory, P.W. McKenty, S. Skupsky, Phys. Plasmas **12**, 042703 (2005).
[10] V.N. Goncharov, J.P. Knauer, P.W. McKenty, P.B. Radha, T.C. Sangster, S. Skupsky, R. Betti, R.L. McCrory, D.D Meyerhofer, Phys. Plasmas **10**, 1906 (2003).
[11] T. J. B. Collins, J. P. Knauer, R. Betti, T. R. Boehly, J. A. Delettrez, V. N. Goncharov, D. D. Meyerhofer, P. W. McKenty, S. Skupsky, R.P.J. Town, Phys. Plasmas **11**, 1569 (2004);
[12] R. Betti, W. Theobald, C.D. Zhou, K.S. Anderson, P.W. McKenty, S. Skupsky, D. Shvarts, V.N. Goncharov, J.A. Delettrez, P.B. Radha, T.C. Sangster, C. Stoeckl, D.D. Meyerhofer, J. Phys.: Conf. Ser. **112**, 022024 (2008).
[13] L.J. Perkins, R. Betti, K.N. LaFortune, W.H. Williams, Phys. Rev. Lett. **103**, 045004 (2009).
[14] A.I. Nikitenko, S.M. Tolokonnikov, R. Cook, Fusion Tech. **31**, 388 (1997).
[15] A. Nikroo, J. Bousquet, R. Cook, B.W. Mcquillan, R. Paguio, M. Takagi, Fusion Sci. Tech. **45**, 165 (2004).
[16] See EPAPS Document No. E-PHPAEN-8-992105 for "Analysis of intensity structure of the ISI model in the FAST2D hydrocode" by A. J. Schmitt. This document may be retrieved via the EPAPS homepage http:// www.aip.org/pubservs/epaps.html or from ftp.aip.org in the directory /epaps/.
[17] R.H. Lehmberg, S.P. Obenschain, Opt. Commun **46**, 27 (1983).